Yang et al. *Zool. Res.* 2025, 46(2): 325−338
https://doi.org/10.24272/j.issn.2095-8137.2024.278
https://cstr.cn/32248.14.zr.2024.278

ZR | Zoological Research

Article Open Access

Dynamic alterations in bacterial and fungal microbiome and inflammatory cytokines following SRV-8 infection in cynomolgus monkeys

Yun-Peng Yang[1,2,3,4,#,*], Li-Bing Xu[1,2,#], Yong Lu[4], Jing Wang[4], Yan-Hong Nie[3,4], Qiang Sun[3,5]

[1] *Jiangsu Co-innovation Center for Prevention and Control of Important Animal Infectious Diseases and Zoonoses*, *College of Veterinary Medicine*, *Yangzhou University*, *Yangzhou*, *Jiangsu* 225009, *China*

[2] *Institute of Comparative Medicine*, *Yangzhou University*, *Yangzhou*, *Jiangsu* 225009, *China*

[3] *Shanghai Center for Brain Science and Brain-Inspired Technology*, *Shanghai* 201602, *China*

[4] *Institute of Neuroscience*, *CAS Key Laboratory of Primate Neurobiology*, *State Key Laboratory of Neuroscience*, *CAS Center for Excellence in Brain Science and Intelligence Technology*, *Chinese Academy of Sciences*, *Shanghai* 200031, *China*

[5] *Key Laboratory of Genetic Evolution* & *Animal Models*, *Chinese Academy of Sciences*, *Kunming*, *Yunnan* 650201, *China*

ABSTRACT

While viral infections can disturb the host gut microbiome, the dynamic alterations in microbial composition following infection remain poorly characterized. This study identified SRV-8-infected monkeys and classified them into five groups based on infection progression. 16S rRNA amplicon sequencing revealed significant alterations in the relative and inferred absolute abundance of bacterial genera *UCG-002*, *Agathobacter*, *Coprococcus*, and *Holdemanella* during the early stage of SRV-8 infection, coinciding with provirus formation. These microbial shifts were accompanied by functional modifications in bacterial communities at the same stage. In contrast, ITS amplicon sequencing indicated no significant differences in fungal composition between healthy wild-type and SRV-8-infected monkeys. Spearman correlation analyses demonstrated close interactions between intestinal bacteria and fungi following SRV-8 infection. Additionally, SRV-8 seropositive groups exhibited significantly elevated mRNA expression levels of pro-inflammatory (*TNF-α*, *IFN-γ*, *IL-1β*, and *IL-6*) and anti-inflammatory (*IL-10*) cytokine genes, highlighting close associations between inflammatory cytokines and immune responses. Overall, these findings provide a comprehensive characterization of bacterial and fungal microbiota dynamics and inflammatory cytokine responses associated with SRV-8 infection, clarifying the pathobiological mechanisms underlying SRV-8 infection from the perspective of the gut microbiome.

Keywords: Cynomolgus monkeys; SRV-8 infection; Dynamic alterations; Bacterial and fungal microbes; Inflammatory cytokines

INTRODUCTION

Accumulating evidence indicates that viral infections significantly alter gut microbiome composition, influencing host-pathogen interactions and disease progression. For instance, HIV infection is associated with an increased abundance of *Prevotella* and a reduced prevalence of *Bacteroides* in the gut microbiota (Chen et al., 2024b). Similarly, chikungunya virus-infected mosquitoes exhibit elevated levels of *Gluconobacter* in the midgut compared to non-infected counterparts (Siriyasatien et al., 2024). Respiratory syncytial virus infection alters gut microbial composition through IL-22-induced overexpression of *RegⅢγ* (Liu et al., 2024), while severe acute respiratory syndrome coronavirus 2 (SARS-CoV-2) infection affects gut microbiota composition over the course of infection (Sencio et al., 2022). Beyond these compositional shifts, the gut microbiota plays a key role in viral pathogenesis. For example, SARS-CoV-2-induced gut microbial alterations increase systemic inflammation and contribute to pathological injury in infected rhesus monkeys (*Macaca mulatta*) (Chen et al., 2024a). Although virus-induced microbiome changes have been

Received: 08 November 2024; Accepted: 03 December 2024; Online: 04 December 2024

Foundation items: This work was supported by the National Science and Technology Innovation 2030 Major Program (2021ZD0200900), National Key Research and Development Program of China (2022YFF0710901), National Natural Science Foundation of China (82021001, 31825018), Biological Resources Program of the Chinese Academy of Sciences (KFJ-BRP-005), 111 Project D18007, and a Project Funded by the Priority Academic Program Development of Jiangsu Higher Education Institutions (PAPD)

[#]Authors contributed equally to this work

*Corresponding author, E-mail: ypyang@yzu.edu.cn

investigated, little is known about the specific dynamics of gut microbial alterations following viral infection.

To date, research on the gut microbiome has largely focused on bacterial and fungal communities, both of which are critical for host health. Bacterial dysbiosis is implicated in a range of diseases, including gastric disorders, cardiovascular disease, liver pathology, immune dysfunction, and neurodegenerative conditions (Han et al., 2024; Hsiao et al., 2013; Lee et al., 2024; Liu et al., 2023b; Qian et al., 2023; Vieira & Baumert, 2024). Likewise, fungal dysbiosis contributes to the development of alcoholic liver disease, allergic airway disorders, and gut colitis (Iliev et al., 2012; Jain et al., 2021; Wheeler et al., 2016; Yang et al., 2017). Given their fundamental roles in host physiology and disease, it is essential to characterize the alternations in bacterial and fungal communities following viral infection to better understand their contribution to disease pathogenesis.

Non-human primates (NHPs) serve as excellent models for biomedical research and clinical applications due to their close genetic, physiological, and behavioral resemblance to humans. NHPs are natural hosts for various retroviruses, including gibbon-ape leukemia virus (GaLV) (Reitz et al., 1979), simian sarcoma virus (Ogura, 1980), simian T-lymphotropic virus (STLV) (van der Kuyl, 2021), simian immunodeficiency virus (SIV) (Bruce et al., 2018), simian type D retrovirus (SRV) (Zhu et al., 2020), simian foamy virus (SFV) (Dynesen et al., 2023), and rhesus macaque rhadinovirus (RRV) (Estep et al., 2020). Among these, SRV, a type D retrovirus, is prevalent in long-tailed macaques (*Macaca fascicularis*) and rhesus macaques (Daniel et al., 1984; Marx et al., 1984; Xu et al., 2023).

SRV infection progresses through three distinct stages: provirus formation, viral particle release, and antibody production. Initially, SRV reverse transcriptase synthesizes complementary DNA (cDNA) from viral RNA, which integrates into the host genome to establish provirus formation. Subsequently, viral particles and SRV-8-specific antibodies become detectable. SRV infection not only induces AIDS-like symptoms in hosts (Lerche, 2010) but also compromises immune function by suppressing lymphocyte activity and reducing immunoglobulin production (Yee et al., 2016). To date, multiple SRV subtypes (SRV-1 to SRV-8) have been isolated from macaques (Grant et al., 1995; Klatzmann et al., 1984; Koide et al., 2019; Lerche, 2010; Maul et al., 1986; Osborn et al., 1984; Zao et al., 2011). While the pathogenicity and immunogenicity of SRV-1–5 have been extensively characterized, recent findings from our laboratory indicate that SRV-8, a recently identified subtype, also induces severe pathogenicity and immune dysregulation in cynomolgus monkeys (Xu et al., 2023). However, the underlying pathobiological mechanisms of SRV-8 infection remain unclear, and its potential interactions with the gut microbiome are largely unexplored.

To investigate gut microbiome alternations associated with SRV-8 infection, SRV-8-infected cynomolgus monkeys were identified and categorized into five groups based on infection progression. Notably, bacterial composition exhibited significant changes in infected monkeys, whereas fungal genera showed no significant differences between wild-type and SRV-8-infected individuals. Further analysis revealed close interactions between intestinal bacteria and fungi following infection. Additionally, SRV-8 seropositive groups displayed increased expression of both pro-inflammatory and anti-inflammatory cytokines, highlighting the immunological impact of SRV-8 infection.

MATERIALS AND METHODS

Animals

Cynomolgus monkeys housed at the Non-Human Primate Facility of the Center for Excellence in Brain Science and Intelligent Technology were maintained on a commercial monkey diet (Anmufei, Suzhou, China), provided twice daily at 0800h and 1500h (30 g/kg per monkey), with free access to municipal water. To supplement vitamins and essential nutrients, monkeys received a daily ration of fresh fruit and vegetables (100 g per monkey) at 1000h. All animals were individually housed for at least two months before the study and had no prior exposure to antibiotics.

Ethics statement

All experimental protocols were approved by the Animal Care Committee at the CAS Center for Excellence in Brain Science and Intelligence Technology, Chinese Academy of Sciences (No. ION-2019043R01).

Screening SRV-8-infected monkeys

Female cynomolgus monkeys (9–14 years old) exhibiting clinical signs such as weight loss, anemia, and diarrhea were selected for SRV-8 screening. Detection of provirus, viral particles, and SRV-8-specific antibodies followed the procedures of our previous study (Xu et al., 2023). Age-matched, clinically healthy female monkeys served as controls. At baseline, body weight ranged from 4 to 6 kg across all groups, with no significant differences between groups.

Genomic DNA was extracted from blood samples using a TIANamp Genomic DNA Kit (Tiangen, China) and used as a template for polymerase chain reaction (PCR) amplification. Primers targeting the conserved envelope (ENV) region of SRV-1/2/4/5/8 were designed (Supplementary Table S1). PCR was carried out under the following cycling conditions: 95℃ for 5 min, followed by 35 cycles at 95℃ for 30 s, 57℃ for 30 s, and 72℃ for 30 s. PCR products were cloned into the pMD19-T vector for sequencing, and sequence similarity was analyzed using BLAST.

SRV-8 viral particles were detected by extracting RNA from peripheral blood mononuclear cells (PBMCs) using an RNAprep Pure Blood Kit (Tiangen, China). The RNA was converted to cDNA using HiScript II Q RT SuperMix for quantitative real-time PCR (qPCR) (with gDNA wiper) (Vazyme Biotech, China). qPCR was performed using AceQ qPCR SYBR® Green Master Mix (Vazyme, Q111-02/03, China) to determine the cycle threshold (Ct) of each sample. SRV-8 viral presence was confirmed when Ct<35 (Supplementary Table S1).

For SRV-8 antibody detection, plasma was collected from SRV-8-infected monkeys. Antibody levels were assessed using an SRV Antibody Detection Kit (VRL-China, E-081110), with OD_{405}>0.3 considered indicative of SRV-8 seropositivity.

Based on infection status, SRV-8-infected monkeys were classified into five groups: (1) SRV-P, provirus detected; (2) SRV-P/V, provirus and viral particles detected; (3) SRV-P/V/A, provirus, viral particles, and antibodies detected; (4) SRV-P/A, provirus and antibodies detected; and (5) SRV-A, antibodies detected. Age-matched wild-type (WT) monkeys served as controls. A total of 42 female cynomolgus monkeys (9–14

years old) were included in the study, with the following group distinctions: WT (*n*=7), SRV-P (*n*=7), SRV-P/V (*n*=3), SRV-P/V/A (*n*=7), SRV-P/A (*n*=9), and SRV-A (*n*=9).

Expression analysis of pro-inflammatory and anti-inflammatory cytokine genes

Total RNA was extracted from PBMCs following previously established protocols (Xu et al., 2023). The conversion of RNA to cDNA was achieved using HiScript II Q RT SuperMix for qPCR (with gDNA wiper) (Vazyme, R223). qRT-PCR was performed with AceQ qPCR SYBR® Green Master Mix (Vazyme, Q111-02/03, China). Gene-specific primers are listed in Supplementary Table S1. Relative expression levels of four pro-inflammatory (*TNF-α*, *IFN-γ*, *IL-1β*, and *IL-6*) and two anti-inflammatory (*IL-10* and *IL-17A*) cytokine genes were quantified using *GAPDH* as an internal reference. Fold-change in gene expression for each SRV-8-infected group was determined relative to the WT group.

16S rRNA amplicon sequencing

Microbial genomic DNA was extracted from fecal samples using a PF Mag-Bind Stool DNA Kit (Omega Bio-Tek, USA). The V3–V4 hypervariable region of the 16S rRNA gene was amplified with the primer pair 338F and 806R (Supplementary Table S1). Following PCR amplification, quantified amplicons were pooled and sequenced on the Illumina MiSeq PE300 platform (Illumina, USA). Raw FASTQ files were de-multiplexed using an in-house Perl script, quality-filtered with fastp v.0.19.6 (Chen et al., 2018), and merged using FLASH v.1.2.11 (Magoč & Salzberg, 2011). High-quality sequences were denoised using the DADA2 (Callahan et al., 2016) plugin in the QIIME2 (v.2020.2) (Bolyen et al., 2019), which resolves sequencing errors and generates amplicon sequence variants (ASVs) with single-nucleotide resolution. Taxonomic assignment of ASVs was performed using the Naïve Bayes consensus taxonomy classifier in QIIME2, with reference to the SILVA 16S rRNA database (v.138). 16S rRNA amplicon sequencing-based prediction of gut microbial function was performed using PICRUSt2 (Douglas et al., 2020).

ITS amplicon sequencing

Fungal DNA was extracted from fecal samples using a PF Mag-Bind Stool DNA Kit (Omega Bio-Tek, USA). The ITS1-2 region of the fungal rRNA gene was amplified using primer pair ITS1F/ITS2R (Supplementary Table S1). PCR-amplified products were pooled in equimolar concentrations and sequenced on the Illumina MiSeq PE300 platform (Illumina, USA). Raw FASTQ files were de-multiplexed using an in-house Perl script, quality-filtered by fastp v.0.19.6 (Chen et al., 2018), and merged using FLASH v.1.2.11 (Magoč & Salzberg, 2011). High-quality sequences were denoised using the DADA2 (Callahan et al., 2016) plugin in QIIME2 (v.2020.2) (Bolyen et al., 2019), generating ASVs with single-nucleotide resolution. Taxonomic assignment was performed using the Naïve Bayes consensus taxonomy classifier in QIIME2, referencing the UNITE ITS database (v.8.0) for fungal classification.

Bioinformatic analyses

Bioinformatic analysis of the gut microbiome was performed using the Majorbio Cloud platform (https://cloud.majorbio.com). Alpha diversity metrics, including ACE, Chao, Shannon, and Simpson, and Good's coverage, were calculated using Mothur v.1.30.2 (Schloss et al., 2009). Beta diversity analysis was performed using principal coordinate analysis (PCoA) based on Bray-Curtis dissimilarity in the Vegan v.2.4.3 package.

16S rRNA- and ITS-based qPCR

Absolute quantification of bacterial and fungal communities in fecal samples was measured using 16S rRNA- and ITS-based qPCR assays. Bacterial abundance was assessed using 16S rRNA-specific primers (forward: 5'-AGAGTTTGATCCTGG CTCAG-3'; reverse: 5'-CTGCTGCCTYCCGTA-3'), while fungal abundance was determined using ITS-specific primers (forward: 5'-TCAGACAGCGATGTTTGGTT-3'; reverse: 5'-AAGTTCAGCGGGTACTCCTA-3'). qPCR was performed using the LightCycler 480 II PCR system (Roche) under the following cycling conditions: 95℃ for 5 min, 45 cycles at 95℃ for 10 s, 60℃ for 10 s, and 72℃ for 10 s. Absolute microbial abundance was determined using standard curves generated from pMD18T vector constructs containing full-length *Escherichia coli* 16S rRNA and *Kazachstania pintolopesii* ITS sequences, ensuring normalization across qPCR runs.

Correlation analysis

Spearman correlation analysis was conducted to evaluate associations between the 30 most abundant bacterial and fungal genera across different stages of SRV-8 infection. Hierarchical clustering of bacterial and fungal genera was performed using the average linkage method. Additionally, Spearman correlation analysis was applied to assess relationships between bacterial genera and predicted bacterial functions.

Statistical analysis

Data are expressed as mean±standard error of the mean (SEM). Statistical significance between WT and SRV-8-infected monkeys was analyzed using an unpaired, two-tailed Student's *t*-test. All statistical analyses were conducted using GraphPad.

RESULTS

Identification and stratification of SRV-8-infected cynomolgus monkeys

SRV infection progresses through three distinct stages: provirus formation, viral particle release, and SRV-specific antibody production (Figure 1A). To identify the SRV provirus in monkeys with clinical symptoms such as weight loss, anemia, and diarrhea, the 198 bp ENV region of various SRV subtypes was amplified by PCR in PBMCs (Supplementary Figure S1A). PCR analysis confirmed the presence of the SRV-8 provirus in the SRV-P, SRV-P/V, and SRV-P/V/A groups (Figure 1B), while SRV-1/2/4/5 were undetectable across all groups (Supplementary Figure S1B). These findings indicate that SRV-8 is the predominant SRV subtype circulating in the research facility.

The presence of SRV-8 viral particles and SRV-8-specific antibodies was assessed using reverse transcription-quantitative real-time polymerase chain reaction (RT-qPCR) and enzyme linked immunosorbent assay (ELISA), respectively. As shown in Figure 1C, D, SRV-8 viral particles were detected in the SRV-P/V and SRV-P/V/A groups, while SRV-8-specific antibodies were detected in the SRV-P/V/A, SRV-P/A, and SRV-A groups. In total, 35 SRV-8-infected cynomolgus monkeys were identified in this study, with the following group distributions: SRV-P (*n*=7), SRV-P/V (*n*=3), SRV-P/V/A (*n*=7), SRV-P/A (*n*=9), and SRV-A (*n*=9).

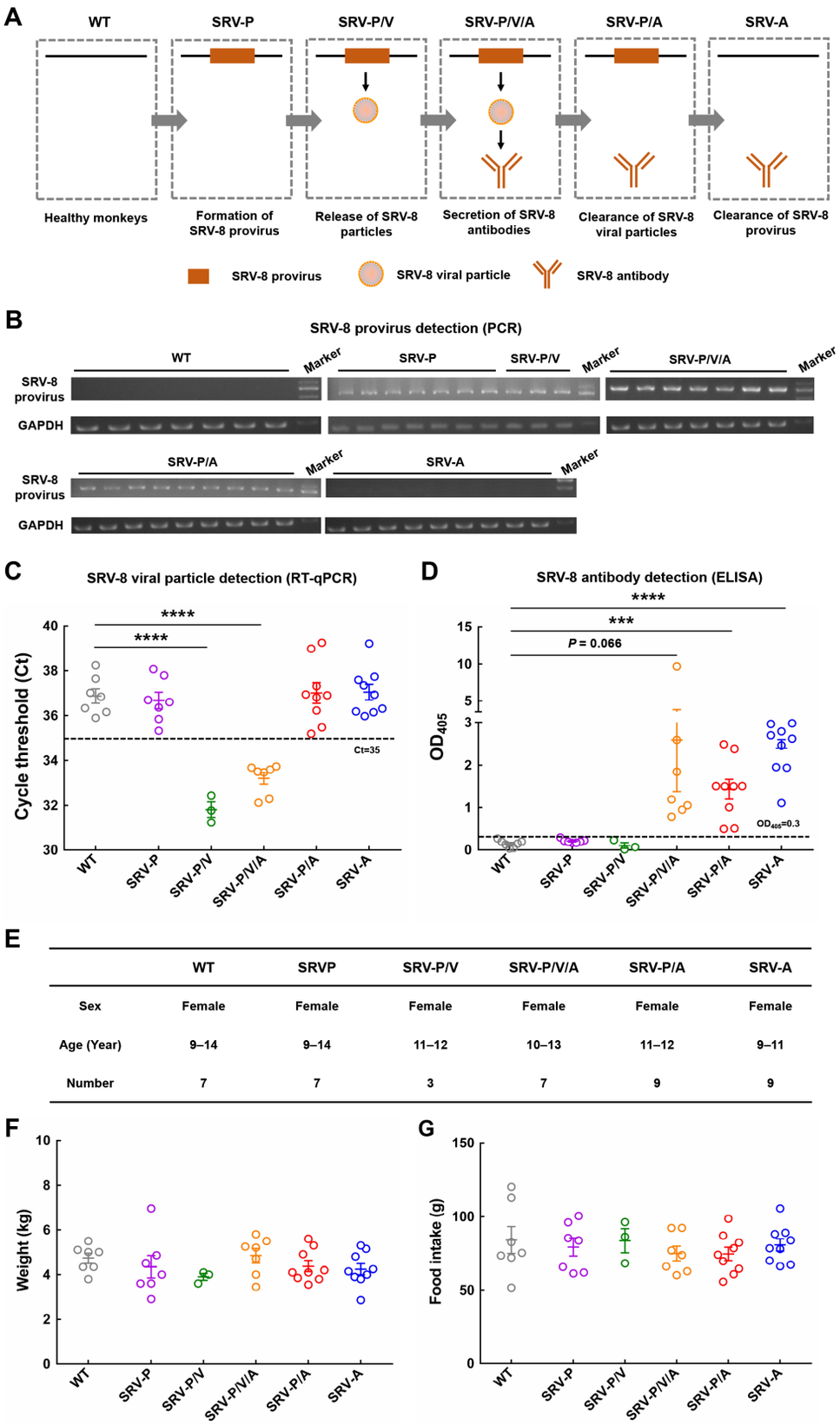

Figure 1 Identification and classification of SRV-8-infected monkeys

A: Schematic illustrating progression of SRV-8 infection and classification of SRV-8-infected monkey groups. B: PCR-based identification of SRV-8 provirus. PCR primers were designed to target conserved envelope (ENV) region of SRV. C: RT-qPCR-based identification of SRV-8 virus. Ct: Cycle threshold. The existence of SRV-8 virus was verified by Ct<35. D: ELISA-based identification of SRV-8 antibodies. The existence of SRV-8 antibodies was verified by OD_{405}>0.3. E: Monkey characteristics across six groups. F, G: Weight (F) and food intake (G) of monkeys in six groups. Data are mean±SEM. Statistical significance between WT and SRV-8-infected monkeys was analyzed using Student's *t*-test (***: P<0.001; ****: P<0.0001).

Additionally, seven WT monkeys were selected as controls (Figure 1E). As shown in Figure 1F, G, no significant differences in body weight or food intake were observed between SRV-8-infected monkeys and WT controls.

Dynamic alterations in bacterial microbes following SRV-8 infection

To investigate gut microbial changes associated with SRV-8 infection, fecal samples from WT and SRV-8-infected monkeys were collected for 16S rRNA amplicon sequencing. Rarefaction analysis standardized sequence counts to 20 121 per sample, achieving an average Good's coverage of 99.58% (Figure 2A). A Venn diagram revealed that 420 ASVs were shared across the WT and five SRV-8-infected monkey groups (Figure 2B). However, alpha diversity indices, including richness (Ace and Chao) and diversity (Shannon and Simpson), showed no significant differences between SRV-8-infected and WT groups (Figure 2C). PCoA of Bray-Curtis distances based on ASVs indicated slight differences in bacterial composition between the WT and SRV-8-infected monkeys (Figure 2D). Notably, compared with the WT group, gut microbial dysbiosis was observed in all five SRV-8-infected groups (Figure 2E). To assess whether SRV-8 infection influenced total bacterial load in the fecal samples of WT and SRV-8-infected monkeys, 16S rRNA qPCR was performed. As shown in Figure 2F, total bacterial load did not differ between the WT and SRV-8-infected groups, suggesting that SRV-8 infection did not impact absolute gut bacterial abundance.

To characterize bacterial community shifts following SRV-8 infection, the relative and inferred absolute abundance of microbiota at both family and genus levels was investigated. Inferred absolute abundance was calculated by multiplying the taxonomic relative abundance of microbiota by total bacterial load in fecal samples. At the family level, Oscillospiraceae and UCG-010 exhibited increased abundance in the SRV-P group, while Lachnospiraceae showed the opposite trend (Figure 2G). Conversely, Monoglobaceae was significantly enriched in the SRV-P, SRV-P/A, and SRV-A groups (Figure 2G). At the genus level, heatmap analysis of the top 30 genera highlighted bacterial differences across groups (Supplementary Figure S2). Notably, *UCG-002* was enriched in the SRV-P group, while *Agathobacter*, *Coprococcus*, and *Holdemanella* were significantly reduced (Figure 3A–D). A distinct reduction in *Sphaerochaeta* was observed exclusively in the SRV-P/A group (Figure 3E), whereas *Monoglobus* was markedly increased in the SRV-P, SRV-P/A, and SRV-A groups (Figure 3F). These findings indicate that SRV-8 infection predominantly alters the bacterial microbiome during the initial provirus formation stage (SRV-P group), indicating early microbial dysbiosis.

To identify microbial taxa associated with SRV-8 infection, linear discriminant analysis (LDA) effect size (LEfSe) was applied to compare bacterial and fungal composition across groups. As shown in Supplementary Figure S3, *Lachnospiraceae_XPB1014_group* was enriched in the WT group. *Rikenellaceae_RC9_gut_group*, *Caldicoprobacter*, *Candidatus_Soleaferrea*, and *unclassified_f_Bacteroidales_RF16_group* were abundant in the SRV-P group, while Rikenellaceae, Proteobacteria, Burkholderiales, Tannerellaceae, and *Parabacteroides* were enriched in the SRV-P/V group. *Human_gut_metagenome_g_Christensenellaceae_R-7_group* was enriched in the SRV-P/V/A group, while Erysipelotrichales and *Coprococcus* were enriched in the SRV-P/A group and *Campylobacter* was abundant in the SRV-A group.

Dynamic alterations in bacterial function following SRV-8 infection

To investigate the functional alterations in gut bacterial communities associated with SRV-8 infection, PICRUSt2 was used to infer metabolic pathways from 16S rRNA sequencing data. Analysis of third-level KEGG pathways revealed distinct functional disruptions in the SRV-P group, with marked reductions in pathways related to starch and sucrose metabolism, amino sugar and nucleotide sugar metabolism, galactose metabolism, the phosphotransferase system, acarbose and validamycin, and glycerolipid metabolism (Figure 4A). In contrast, pathways linked to bacterial chemotaxis, biofilm formation (*Vibrio cholerae*), flagellar assembly, butanoate metabolism, lipoic acid metabolism, and carbon fixation in prokaryotes were enriched in the SRV-P group (Figure 4B). Further analysis indicated that starch and sucrose metabolism, the phosphotransferase system, and glycerolipid metabolism exhibited reduced functional abundance in the SRV-P group, whereas amino sugar and nucleotide sugar metabolism, galactose metabolism, and acarbose and validamycin biosynthesis were decreased in both the SRV-P and SRV-A groups (Figure 4A). Conversely, bacterial chemotaxis, biofilm formation (*Vibrio cholerae*), flagellar assembly, butanoate metabolism, and carbon fixation pathways in prokaryotes were significantly enriched in the SRV-P group, while lipoic acid metabolism was increased in the SRV-P and SRV-P/V groups (Figure 4B).

Correlations between bacterial genera and functional pathways in WT and SRV-P groups

Given the distinct microbial and functional differences between WT and SRV-P groups (Figures 3, 4), Spearman correlation analysis was performed to examine the association between bacterial genera and metabolic functions in these groups. As shown in Supplementary Figure S4, *UCG-002* exhibited strong negative correlations with pathways involved in starch and sucrose metabolism, amino sugar and nucleotide sugar metabolism, galactose metabolism, the phosphotransferase system, acarbose and validamycin, and glycerolipid metabolism but strong positive correlations with bacterial functions related to bacterial chemotaxis, biofilm formation (*Vibrio cholerae*), flagellar assembly, butanoate metabolism, lipoic acid metabolism, and carbon fixation pathways in prokaryotes. Conversely, *Agathobacter*, *Coprococcus*, and *Holdemanella* displayed opposite correlation patterns.

Dynamic alterations in fungal microbiome following SRV-8 infection

To characterize the impact of SRV-8 infection on the gut fungal microbiome, ITS amplicon sequencing was performed on fecal samples collected from WT and SRV-8-infected monkeys. Rarefaction analysis standardized sequence counts to 39 783, achieving an average Good's coverage of 99.99% (Supplementary Figure S5). Analysis of ASVs revealed that only 17 ASVs were shared between the WT and SRV-8-infected monkey groups (Supplementary Figure S6). Alpha diversity metrics, including richness (Ace and Chao) and diversity indices (Shannon and Simpson), showed no significant differences between the WT and SRV-8 infected groups (Figure 5A). Similarly, PCoA based on Bray-Curtis

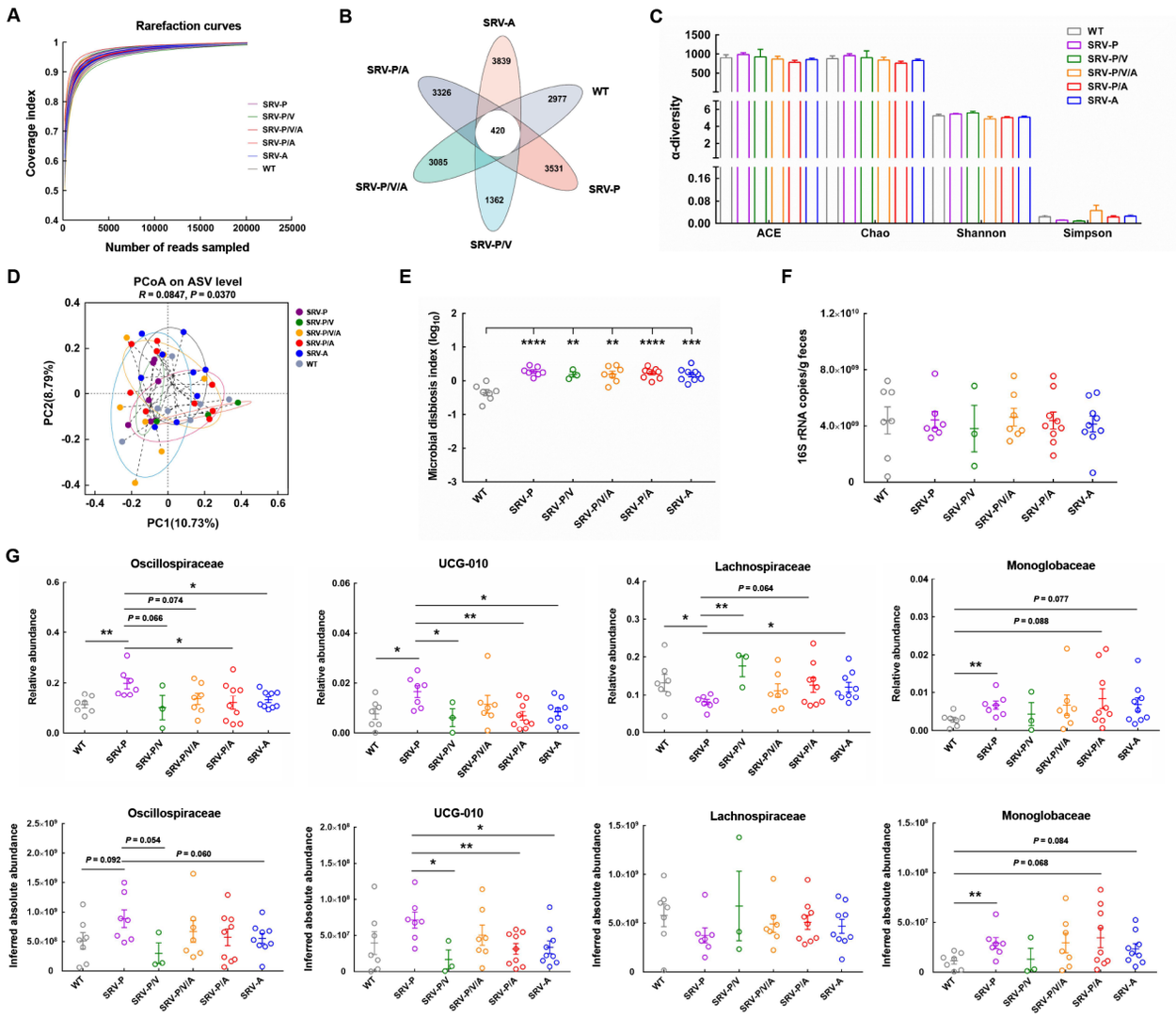

Figure 2 Dynamic alterations in bacterial microbes following SRV-8 infection

A: Coverage index curve of each sample from six monkey groups. B: Number of different ASVs between WT and SRV-8-infected monkey groups. C: Richness (ACE and Chao) and diversity (Shannon and Simpson) of bacterial microbiome between WT and SRV-8-infected monkeys. D: PCoA of Bray-Curtis distances based on ASVs of WT and SRV-8-infected monkeys. Permutational multivariate ANOVA (PERMANOVA) was applied to test differences between groups. E: Comparison of microbial dysbiosis index between WT and SRV-8-infected monkeys. F: Total bacterial load between WT and SRV-8-infected monkeys. G: Relative and inferred absolute abundance of bacterial community between WT and SRV-8-infected monkeys at the family level. Inferred absolute abundance was calculated by multiplying the taxonomic relative abundance of microbiota by the 16S rRNA copy number in fecal samples. Data are mean±SEM. Statistical significance between different monkey groups was analyzed using Student's *t*-test (*: $P<0.05$; **: $P<0.01$; ***: $P<0.001$; ****: $P<0.0001$).

distances indicated that fungal community composition remained largely unchanged across WT and SRV-8-infected monkeys (Figure 5B). However, signs of gut microbial dysbiosis were observed in the SRV-P/V, SRV-P/V/A, and SRV-A groups, suggesting potential fungal perturbations at specific infection stages (Figure 5C).

To determine whether SRV-8 infection influenced total fungal load, ITS-based qPCR was conducted. Notably, no significant changes in absolute fungal abundance were observed across the different infection stages, indicating that SRV-8 infection had minimal impact on fungal colonization dynamics (Figure 5D). Further investigation at the genus level, using heatmap analysis, demonstrated that the fungal microbiome remained largely unaffected by SRV-8 infection (Figure 5E). Consistently, LEfSe analysis identified no significantly enriched fungal taxa distinguishing WT and SRV-8-infected groups, reinforcing the observation that fungal microbiome alterations were negligible in response to SRV-8 infection.

Correlations between relative abundance of bacterial and fungal genera following SRV-8 infection

To characterize bacterial-fungal interactions following SRV-8 infection, the 30 most abundant bacterial and fungal genera from WT and SRV-8-infected monkeys were subjected to Spearman correlation analysis. In WT monkeys, *Kazachstania* was positively correlated with *Phascolarctobacterium* but negatively correlated with *Rikenellaceae_RC9_gut_group*, *Treponema*, and *unclassified_f_Oscillospiraceae*. Furthermore, *Candida* was positively correlated with *Treponema* and *unclassified_f_Oscillospiraceae* (Figure 6A).

In the SRV-P group, correlations between bacterial and fungal taxa shifted, with *Cutaneotrichosporon* negatively

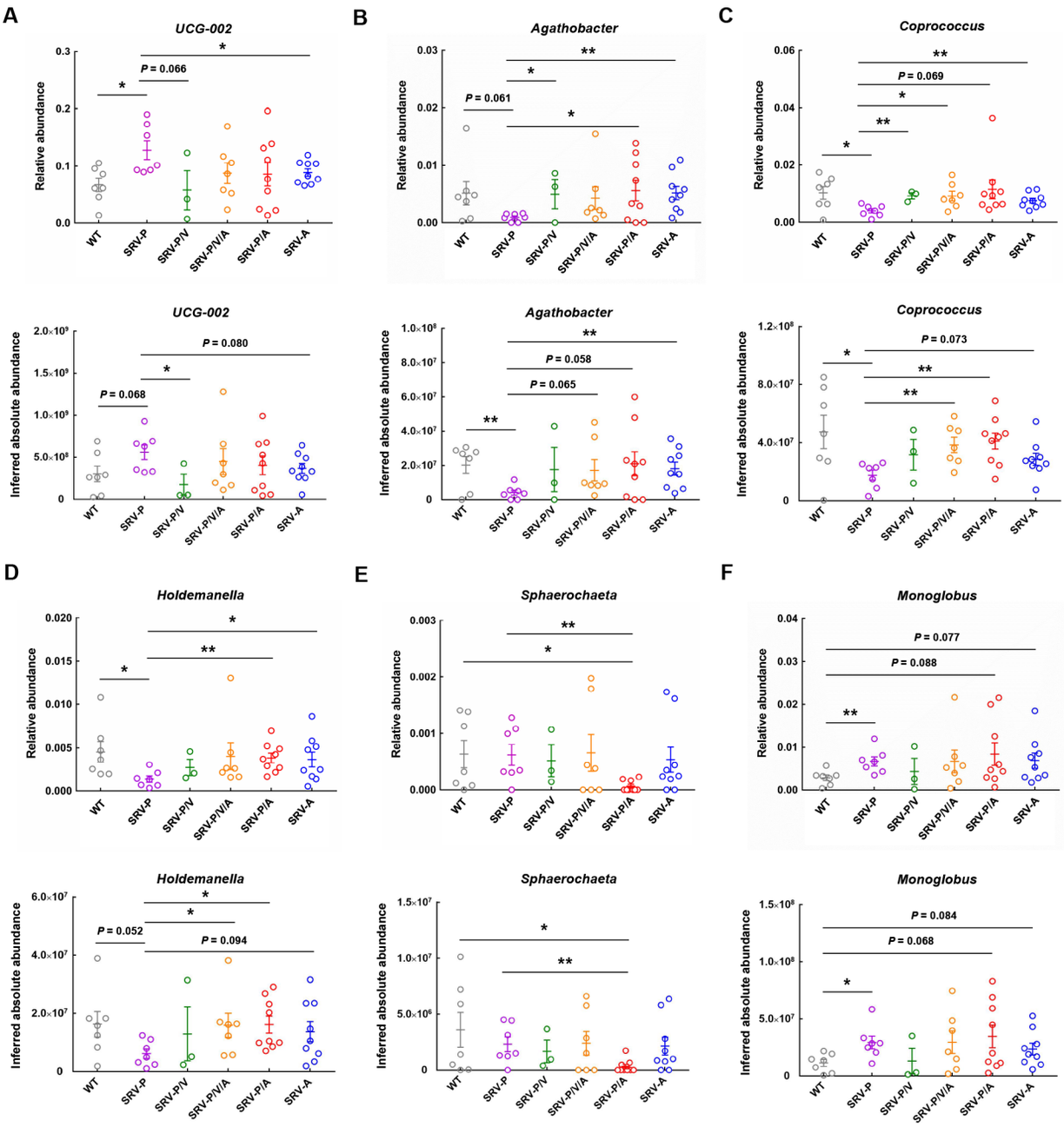

Figure 3 Comparison of bacterial genera between WT and SRV-8-infected monkeys

A–F: Relative and inferred absolute abundance of *UCG-002* (A), *Agathobacter* (B), *Coprococcus* (C), *Holdemanella* (D), *Sphaerochaeta* (E), and *Monoglobus* (F) in WT and SRV-8-infected monkeys. Data are mean±SEM. Statistical significance between different monkey groups was analyzed using student's *t*-test (*: $P<0.05$; **: $P<0.01$).

correlated with *Coprococcus*, while *Cladosporium* showed a negative correlation with bacterial genera *Prevotella_9* and *unclassified_f_Prevotellaceae*. In contrast, *Bullera* and *Papiliotrema* were positively correlated with *Phascolarctobacterium* and *UCG-003* but negatively correlated with *unclassified_f_Oscillospiraceae* (Figure 6B).

In the SRV-P/V group, the fungal genus *Kazachstania* was positively correlated with *Dorea* and *Phascolarctobacterium* but negatively correlated with *Anaerostipes*, *Coprococcus*, *Dialister*, *Rikenellaceae_RC9_gut_group*, *Streptococcus*, *UCG-005*, *unclassified_c_Bacilli*, and *unclassified_f_Muribaculaceae*; In contrast, *Candida*, *Apiotrichum*, and *Wickerhamiella* showed the opposite correlation pattern. Furthermore, *Acremonium* and *Vishniacozyma* were positively correlated with *Ligilactobacillus*, *Treponema*, and *UCG-003* but negatively correlated with *Ruminococcus*, *Subdoligranulum*, *Eubacterium_ruminantium_group*, and *unclassified_f_Lachnospiraceae*. However, the fungal genera *Solicoccozyma* and *Filobasidium* showed the opposite trend with *Acremonium* and *Vishniacozyma* (Figure 6C).

In the SRV-P/V/A group, the fungal genus *Acremonium* was positively correlated with the bacterial genus *NK4A214_group* but negatively correlated with *Anaerostipes*, *Blautia*, *Faecalibacterium*, *Oribacterium*, *Prevotella*, *Prevotella_9*, and *unclassified_f_Lachnospiraceae*. The fungal genus *Botryotrichum* was positively correlated with *Eubacterium_ruminantium_group* and *unclassified_c_Bacilli* but negatively correlated with *Alloprevotella*, *Anaerostipes*,

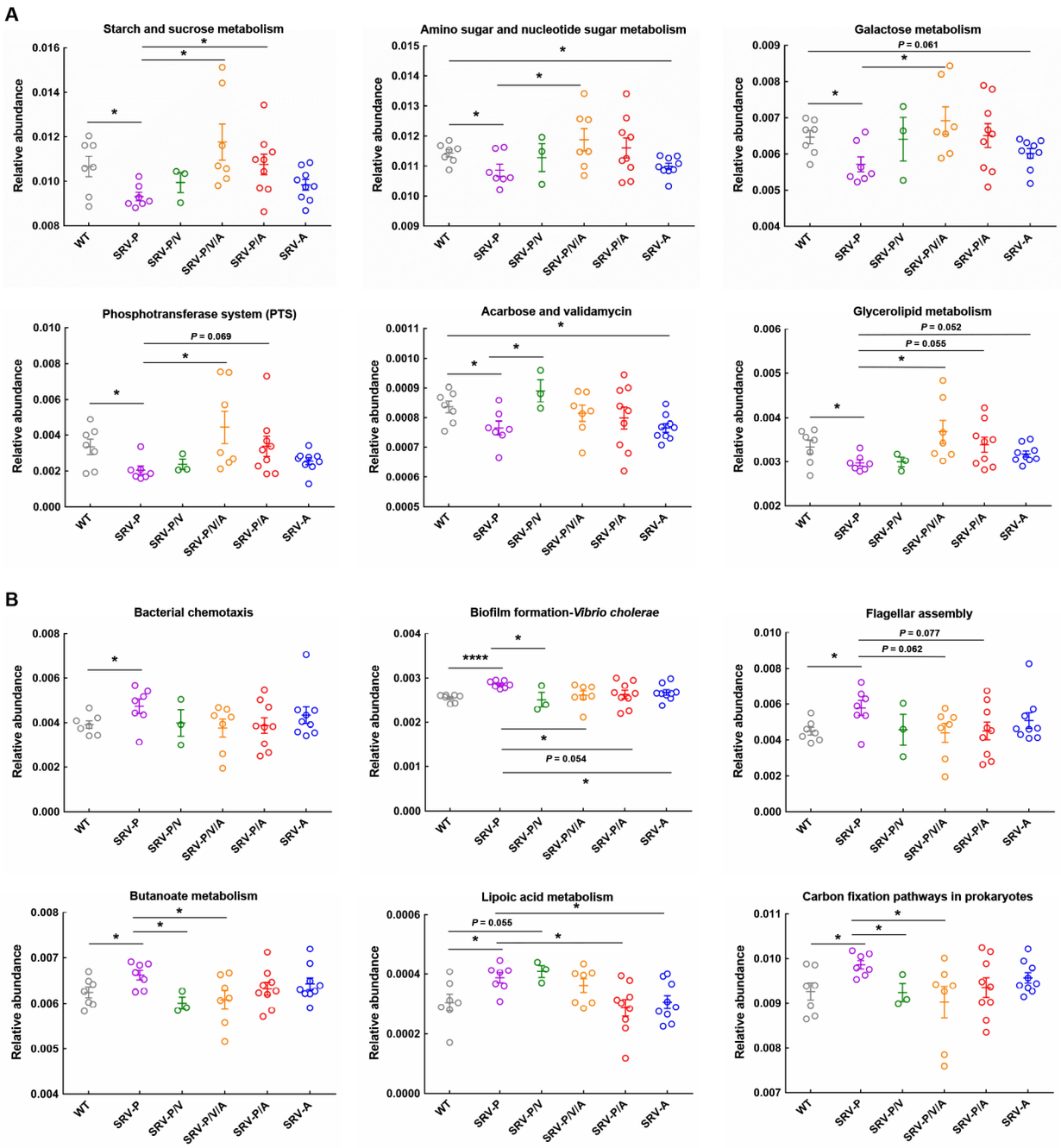

Figure 4 PICRUSt2-predicted KEGG pathway enrichment of intestinal bacteria between WT and SRV-8-infected monkeys

A: Relative abundance of third-level KEGG pathways that decreased in the SRV-P group. B: Relative abundance of third-level KEGG pathways that increased in the SRV-P group. Data are mean±SEM. Statistical significance between different monkey groups was analyzed using student's *t*-test (*: $P<0.05$; ****: $P<0.0001$).

Faecalibacterium, *Oribacterium*, *Prevotella*, *Prevotella_9*, *Rikenellaceae_RC9_gut_group*, *UCG-003*, *unclassified_f_Erysipelotrichaceae*, and *unclassified_f_Lachnospiraceae*. Furthermore, *Wickerhamiella* was negatively correlated with *Agathobacter*, *Blautia*, *Coprococcus*, *Faecalibacterium*, and *unclassified_f_Lachnospiraceae* (Figure 6D).

In the SRV-P/A group, the fungal genus *Sarocladium* was positively correlated with bacterial genera *Blautia* and *Dialister* but negatively correlated with *Ligilactobacillus*, *Prevotellaceae_UCG-003*, *UCG-005*, and *unclassified_c_Clostridia*. The fungal genus *unclassified_k_Fungi* was positively correlated with *Blautia*, *Coprococcus*, *Faecalibacterium*, and *Subdoligranulum* but negatively correlated with *Christensenellaceae_R-7_group*, *NK4A214_group*, *Rikenellaceae_RC9_gut_group*, *Ruminococcus*, *UCG-002*, *UCG-003*, *unclassified_c_Clostridia*, *unclassified_f_Muribaculaceae*, and *unclassified_f_Oscillospiraceae* (Figure 6E).

In the SRV-A group, the fungal genus *Apiotrichum* was positively correlated with the bacterial genus *Ruminococcus* but negatively correlated with *UCG-003* and *UCG-005*. *Vishniacozyma* was positively correlated with bacterial genera *Christensenellaceae_R-7_group*, *Streptococcus*, and *unclassified_c_Clostridia* but negatively correlated with *Alloprevotella* and *Prevotella*. Furthermore, *unclassified_k_Fungi* was positively correlated with *Prevotellaceae_UCG-*

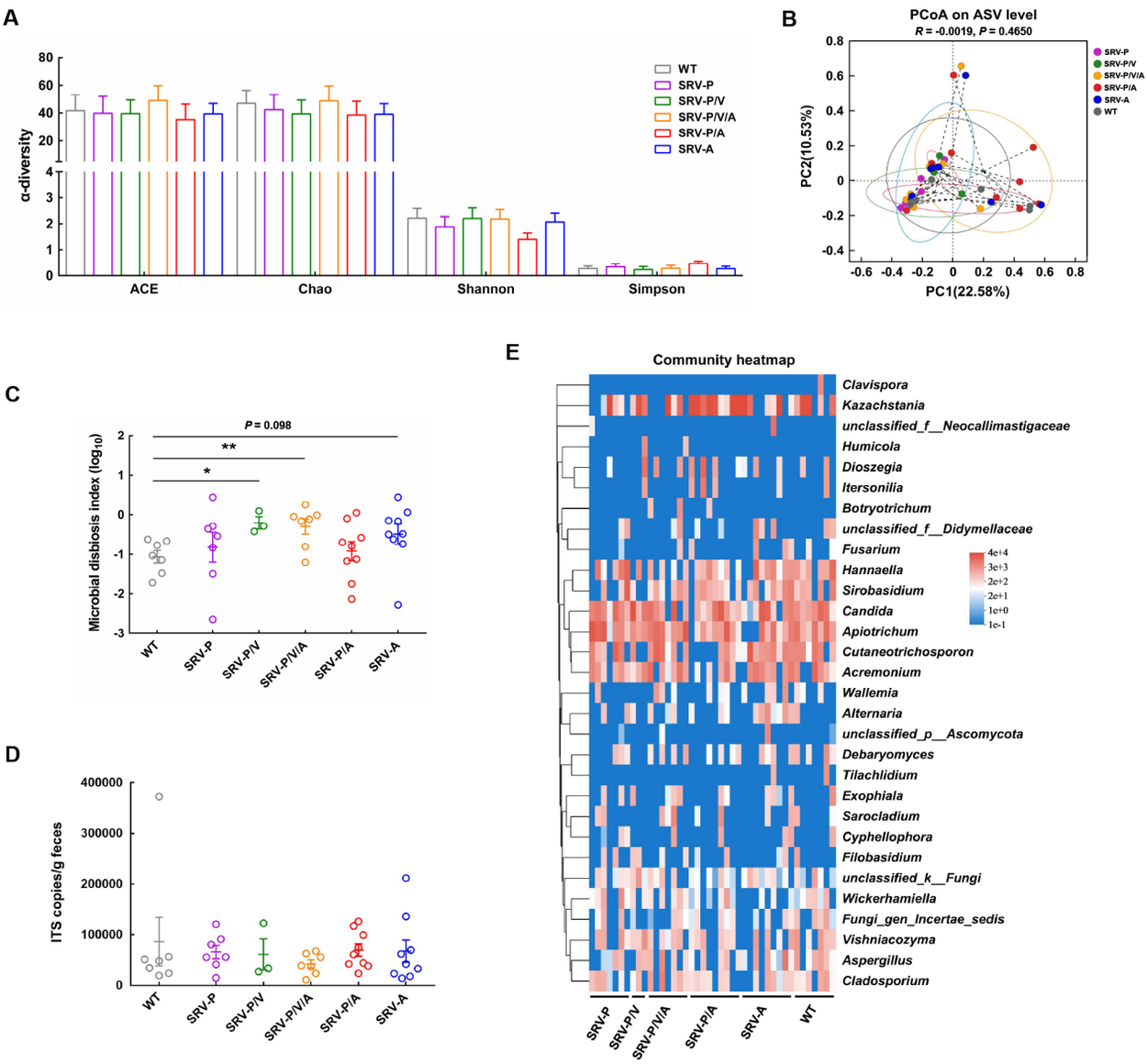

Figure 5 Dynamic alterations in fungal microbes following SRV-8 infection

A: Richness (ACE and Chao) and diversity (Shannon and Simpson) of fungal microbiome in WT and SRV-8-infected monkeys. B: PCoA of Bray-Curtis distances based on ASVs of WT and SRV-8-infected monkeys. Permutational multivariate ANOVA (PERMANOVA) was used to test differences between groups. C: Comparison of microbial dysbiosis index between WT and SRV-8-infected monkeys. D: Total fungal load in WT and SRV-8-infected monkey groups. E: Community heatmap of 30 most abundant fungal genera between WT and SRV-8-infected monkeys. Data are mean±SEM. Statistical significance between WT and SRV-8-infected monkeys was analyzed using Student's *t*-test (*: $P<0.05$; **: $P<0.01$).

003, *Rikenellaceae_RC9_gut_group*, *UCG-003*, and *unclassified_f_Muribaculaceae* but negatively correlated with *Agathobacter*, *Blautia*, *Faecalibacterium*, and *unclassified_f_Lachnospiraceae* (Figure 6F).

Alterations in inflammatory cytokine gene expression following SRV-8 infection

Inflammatory cytokines play a critical role in disease progression and prognosis (Hu et al., 2022; Tong et al., 2022; Wang et al., 2018). To evaluate the impact of SRV-8 infection on immune regulation, RT-qPCR was used to quantify the relative expression levels of pro-inflammatory and anti-inflammatory cytokine genes in PBMCs from WT and SRV-8-infected monkeys. As shown in Figure 7A, the expression levels of pro-inflammatory cytokine genes *TNF-α*, *IFN-γ*, *IL-1β*, and *IL-6* remained low in the WT, SRV-P, and SRV-P/V groups but were markedly elevated in the SRV-P/V/A, SRV-P/A, and SRV-A groups. Similarly, the anti-inflammatory cytokine gene *IL-10* was markedly increased in the SRV-P/V/A, SRV-P/A, and SRV-A groups (Figure 7B). In contrast, no significant difference in *IL-17A* expression was observed between the WT and SRV-8-infected groups (Figure 7B).

DISCUSSION

The pathogenic outcomes of viral infections are shaped by complex interactions among the virus, intestinal microbiota, and host immune factors. While previous studies have explored the association between viral infections and gut microbial disturbances, the dynamic progression of microbial alterations following infection remains poorly understood. This study specifically investigated SRV-8, a retrovirus responsible for severe pathogenicity and immune dysregulation in captive cynomolgus monkeys (Xu et al., 2023) and provided a comprehensive characterization of bacterial and fungal

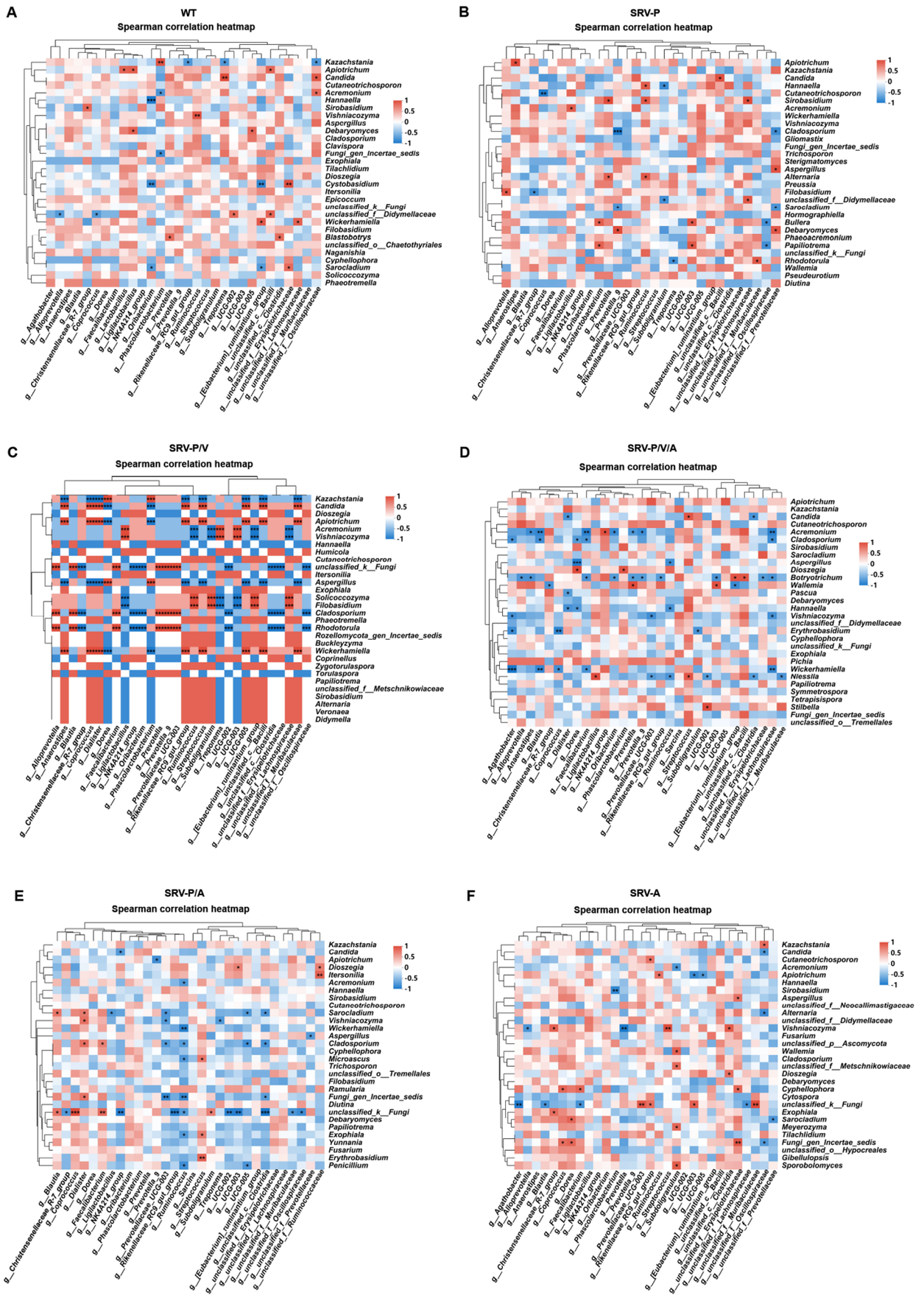

Figure 6 Correlations between the 30 most abundant bacterial and fungal genera in WT (A), SRV-P (B), SRV-P/V (C), SRV-P/V/A (D), SRV-P/A (E), and SRV-A (F) groups

Average linkage method was used to cluster bacteria and fungi. Associations were analyzed using Spearman correlation.

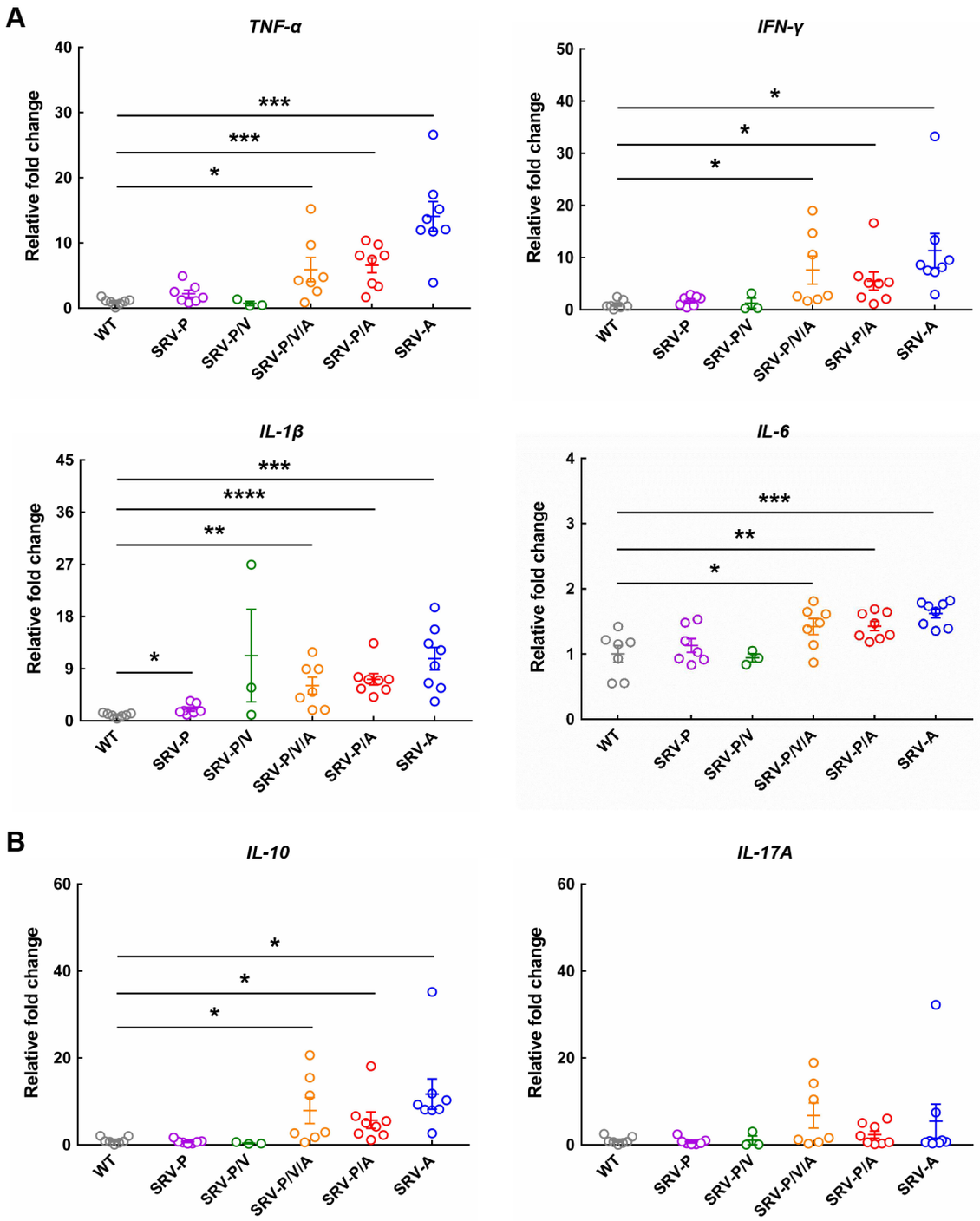

Figure 7 mRNA expression levels of pro-inflammatory (A) and anti-inflammatory cytokine (B) genes in PBMCs following SRV-8 infection

Relative expression levels of four pro-inflammatory (*TNF-α*, *IFN-γ*, *IL-1β*, and *IL-6*) and two anti-inflammatory (*IL-10* and *IL-17A*) cytokine genes were calculated by normalization to *GAPDH*. Relative fold-change of these genes in the SRV-P, SRV-P/V, SRV-P/V/A, SRV-P/A, and SRV-A groups was calculated relative to the WT group. Data are mean±SEM. Statistical significance between WT and SRV-8-infected monkeys was analyzed using student's *t*-test (*: $P<0.05$; **: $P<0.01$; ***: $P<0.001$; ****: $P<0.0001$).

microbiome shifts alongside inflammatory cytokine responses throughout different stages of infection.

To systematically evaluate microbial alterations, SRV-8-infected monkeys were categorized into five groups based on infection progression. Notably, only three monkeys were identified in the SRV-P/V group, in contrast to the WT, SRV-P, SRV-P/V/A, SRV-P/A, and SRV-A groups, (Figure 1E). This scarcity suggests that the secretion of SRV-8-specific antibodies may be too rapid for detection in SRV-P/V monkeys. This hypothesis warrants further verification through expanded screening of SRV-8-infected monkeys in future investigations. Consequently, the small sample size of the SRV-P/V group represents a limitation in this study, highlighting the need for broader cohort analyses to capture the full spectrum of SRV-8 infection dynamics.

16S rRNA amplicon sequencing revealed significant alterations in the gut bacterial microbiome of SRV-8-infected monkeys, with the most pronounced changes occurring in the

SRV-P group (Figure 3). These findings indicate that bacterial communities actively participate in the early stages of SRV-8 infection, potentially influencing disease progression. Among the differentially affected bacterial genera, *UCG-002* exhibited a marked increase in the SRV-P group (Figure 3A). Previous studies have identified *UCG-002* as an opportunistic taxon enriched in early-stage chronic kidney disease patients with hyperuricemia, where it is associated with detrimental effects on host health (Liu et al., 2023a). To further explore the impact of *UCG-002* in SRV-8-infected monkeys, correlation analysis was performed between its relative and inferred absolute abundance and the functional composition of the gut microbiome (Supplementary Figure S7A, B). This analysis revealed a negative correlation between *UCG-002* abundance and microbial pathways involved in carbohydrate metabolism, including starch and sucrose metabolism, amino sugar and nucleotide sugar metabolism, galactose metabolism, and the phosphotransferase system. Conversely, *UCG-002* was positively correlated with biofilm formation of *Vibrio cholerae*, a known enteropathogen. These findings suggest that enrichment of *UCG-002* in SRV-8-infected monkeys may disrupt nutrient utilization in the gut microbiome, potentially altering microbial community stability. Such dysbiosis may compromise host resistance to pathogenic colonization, thereby exacerbating susceptibility to viral infections such as SRV-8.

The SRV-P monkey group exhibited a notable decline in several bacterial genera with well-documented roles in host health. *Agathobacter*, a butyrate-producing genus, is down-regulated in patients diagnosed with cerebral ischemic stroke (Bao et al., 2024), inflammatory bowel disease with extraintestinal manifestations (Hertz et al., 2024), and chronic spontaneous urticaria with vitamin D3 insufficiency (Yang et al., 2024b). Similarly, *Holdemanella* is negatively correlated with various diseases, including Alzheimer's disease (Ning et al., 2024), Crohn's disease, and ulcerative colitis (Wang et al., 2024a). Additionally, *Coprococcus* exerts beneficial effects in endurance athletes by improving their overall health (Duan et al., 2024) and has been shown to maintain intestinal barrier function in hens (Wang et al., 2024b). The depletion of these beneficial bacterial genera in SRV-8-infected monkeys suggests a disruption in microbial equilibrium that may further exacerbate SRV-8 infection.

In contrast to the bacterial microbiome, ITS amplicon sequencing indicated that fungal community composition remained largely unaltered between the WT and SRV-8-infected monkeys, regardless of infection stage (Figure 5). This stability is consistent with previous findings that fungi constitute a minor fraction of the gut microbiota, with many highly abundant fungal genera, such as *Aspergillus*, *Talaromyces*, and *Wallemia*, exhibiting only slight variation under external influences, including circadian rhythm fluctuations (Yang et al., 2024a). Given these observations, it is plausible that the fungal microbiome exhibits greater resistance to external perturbations than the bacterial microbiome, explaining its apparent stability during SRV-8 infection.

Our previous study demonstrated that B cell and natural killer (NK) cell percentages were reduced in the SRV-P group but returned to baseline levels in the three seropositive groups (Xu et al., 2023). In parallel, immunity-related gene expression was also down-regulated in the SRV-P group (Xu et al., 2023). Consistent with these immunological changes, the present study revealed significant disruptions in the gut bacterial microbiome within the SRV-P group (Figure 3), highlighting the close associations between the microbial composition and immune function during the early stage of SRV-8 infection.

Further analysis of bacterial functional profiles in SRV-P monkeys revealed a marked reduction in pathways associated with carbohydrate metabolism, including starch and sucrose metabolism, amino sugar and nucleotide sugar metabolism, galactose metabolism, the phosphotransferase system, and acarbose and validamycin (Figure 4A), while *Vibrio cholerae* biofilm formation was significantly enriched (Figure 4B). These findings suggest that functional dysbiosis in the bacterial microbiome may facilitate SRV-8 intestinal colonization. Additionally, our previous study found that genes involved in carbohydrate and amino acid metabolism were down-regulated in PBMCs of SRV-P monkeys (Xu et al., 2023). This metabolic disruption may limit nutrient availability for host immune cells, further exacerbating immune suppression and increasing susceptibility to SRV-8 infection.

To investigate the connection between specific bacterial functions and inflammatory cytokines/immune responses, correlation analysis was performed. Results showed that the average relative abundance of lipoic acid metabolism was negatively correlated with average OD_{405} values (a parameter for SRV-8 antibody detection) and average relative fold-changes of *TNF-α*, *IFN-γ*, *IL-6*, and *IL-10* (Supplementary Figure S8). Lipoic acid is a dietary supplement with well-documented antioxidant and anti-inflammatory properties (Ruchika et al., 2024). Studies have reported that lipoic acid can attenuate kidney edema and decrease pro-inflammatory cytokines, particularly TNF-α and IL-6, in renal tissues (Skibska et al., 2023). Furthermore, it has been shown to suppress innate immune cell infiltration and activation in visceral adipose tissue of obese insulin-resistant mice (Deiuliis et al., 2011). Collectively, these findings suggest that lipoic acid metabolism is closely associated with inflammatory cytokine regulation and immune function, potentially influencing the progression of SRV-8 infection through its effects on systemic inflammation and immune homeostasis.

CONCLUSIONS

This study provided a detailed characterization of gut bacterial and fungal alterations following SRV-8 infection in cynomolgus monkeys. The bacterial microbiome was significantly disrupted in SRV-8-infected monkeys, whereas the fungal community remained largely unchanged compared to WT controls. Further analysis revealed close interactions between intestinal bacteria and fungi following SRV-8 infection. Additionally, pro- and anti-inflammatory cytokine expression levels were elevated in SRV-8-seropositive groups, implying that inflammatory responses may contribute to viral clearance by affecting immune activity in SRV-8 infected monkeys. Collectively, this study enhances our understanding of SRV-8-induced microbial dysbiosis and immune activation, offering insights into the pathobiological mechanisms of SRV-8 infection from a gut microbiome perspective.

DATA AVAILABILITY

The 16S rRNA and ITS amplicon sequencing data were deposited in the Sequence Read Archive of NCBI (Accession No. SRP509920 and SRP511147) and uploaded to the Science Data Bank database (DOI: 10.57760/sciencedb.j00139.00138) and Genome Sequence Archive database (PRJCA033105).

SUPPLEMENTARY DATA

Supplementary data to this article can be found online.

COMPETING INTERESTS

The authors declare that they have no competing interests.

AUTHORS' CONTRIBUTIONS

Y.P.Y. and Q.S. designed the study. L.B.X., Y.L., J.W., and Y.H.N. performed the experiments. Y.P.Y. and L.B.X. analyzed the data. Y.P.Y. and L.B.X. wrote the manuscript. Q.S. revised the manuscript. All authors read and approved the final version of the manuscript.

ACKNOWLEDGMENTS

We acknowledge the members of Songjiang Non-Human Primate Facility of the CAS Center for Excellence in Brain Science and Intelligence Technology, especially the veterinary team for their invaluable assistance in animal experiments.

REFERENCES

Bao WX, Sun Y, Wang JH, et al. 2024. Relationship between the gut microbiota and neurological deficits in patients with cerebral ischemic stroke. *Neurorehabilitation and Neural Repair*, **38**(7): 527–538.

Bolyen E, Rideout JR, Dillon MR, et al. 2019. Reproducible, interactive, scalable and extensible microbiome data science using QIIME 2. *Nature Biotechnology*, **37**(8): 852–857.

Bruce AG, Barcy S, Staheli J, et al. 2018. Experimental co-transmission of Simian Immunodeficiency Virus (SIV) and the macaque homologs of the Kaposi Sarcoma-Associated Herpesvirus (KSHV) and Epstein-Barr Virus (EBV). *PLoS One*, **13**(11): e0205632.

Callahan BJ, McMurdie PJ, Rosen MJ, et al. 2016. DADA2: high-resolution sample inference from Illumina amplicon data. *Nature Methods*, **13**(7): 581–583.

Chen HY, Wang JB, Ding KY, et al. 2024a. Gastrointestinal microbiota and metabolites possibly contribute to distinct pathogenicity of SARS-CoV-2 proto or its variants in rhesus monkeys. *Gut Microbes*, **16**(1): 2334970.

Chen SF, Zhou YQ, Chen YR, et al. 2018. fastp: an ultra-fast all-in-one FASTQ preprocessor. *Bioinformatics*, **34**(17): i884–i890.

Chen X, Wei JQ, Li Z, et al. 2024b. Dysregulation of gut microbiota-derived neuromodulatory amino acid metabolism in Human Immunodeficiency Virus-associated neurocognitive disorder: an integrative metagenomic and metabolomic analysis. *Annals of Neurology*, **96**(2): 306–320.

Daniel MD, King NW, Letvin NL, et al. 1984. A new type D retrovirus isolated from macaques with an immunodeficiency syndrome. *Science*, **223**(4636): 602–605.

Deiuliis JA, Kampfrath T, Ying Z, et al. 2011. Lipoic acid attenuates innate immune infiltration and activation in the visceral adipose tissue of obese insulin resistant mice. *Lipids*, **46**(11): 1021–1032.

Douglas GM, Maffei VJ, Zaneveld JR, et al. 2020. PICRUSt2 for prediction of metagenome functions. *Nature Biotechnology*, **38**(6): 685–688.

Duan R, Liu Y, Zhang YL, et al. 2024. The impact of exercise on the gut microbiota in middle-aged amateur serious runners: a comparative study. *Frontiers in Physiology*, **15**: 1343219.

Dynesen LT, Fernandez I, Coquin Y, et al. 2023. Neutralization of zoonotic retroviruses by human antibodies: genotype-specific epitopes within the receptor-binding domain from simian foamy virus. *PLoS Pathogens*, **19**(4): e1011339.

Estep RD, Govindan AN, Manoharan M, et al. 2020. Molecular analysis of lymphoid tissue from rhesus macaque rhadinovirus-infected monkeys identifies alterations in host genes associated with oncogenesis. *PLoS One*, **15**(2): e0228484.

Grant RF, Malinak CJ, Wu HN, et al. 1995. PCR amplification and DNA sequencing of SRV-2 from archived tumor tissues. *Virus Research*, **36**(2-3): 187–200.

Han K, Xu J, Xie F, et al. 2024. Engineering strategies to modulate the gut microbiome and immune system. *The Journal of Immunology*, **212**(2): 208–215.

Hertz S, Anderson JM, Nielsen HL, et al. 2024. Fecal microbiota is associated with extraintestinal manifestations in inflammatory bowel disease. *Annals of Medicine*, **56**(1): 2338244.

Hsiao EY, McBride SW, Hsien S, et al. 2013. Microbiota modulate behavioral and physiological abnormalities associated with neurodevelopmental disorders. *Cell*, **155**(7): 1451–1463.

Hu SY, Lee H, Zhao HP, et al. 2022. Inflammation and severe cerebral venous thrombosis. *Frontiers in Neurology*, **13**: 873802.

Iliev ID, Funari VA, Taylor KD, et al. 2012. Interactions between commensal fungi and the C-type lectin receptor Dectin-1 influence colitis. *Science*, **336**(6086): 1314–1317.

Jain U, Ver Heul AM, Xiong SS, et al. 2021. *Debaryomyces* is enriched in Crohn's disease intestinal tissue and impairs healing in mice. *Science*, **371**(6534): 1154–1159.

Klatzmann D, Barré-Sinoussi F, Nugeyre MT, et al. 1984. Selective tropism of lymphadenopathy associated virus (LAV) for helper-inducer T lymphocytes. *Science*, **225**(4657): 59–63.

Koide R, Yoshikawa R, Okamoto M, et al. 2019. Experimental infection of Japanese macaques with simian retrovirus 5. *Journal of General Virology*, **100**(2): 266–277.

Lee SY, Jhun J, Woo JS, et al. 2024. Gut microbiome-derived butyrate inhibits the immunosuppressive factors PD-L1 and IL-10 in tumor-associated macrophages in gastric cancer. *Gut Microbes*, **16**(1): 2300846.

Lerche NW. 2010. Simian retroviruses: infection and disease-implications for immunotoxicology research in primates. *Journal of Immunotoxicology*, **7**(2): 93–101.

Liu JL, Huang YX, Liu N, et al. 2024. The imbalance of pulmonary Th17/Treg cells in BALB/c suckling mice infected with respiratory syncytial virus-mediated intestinal immune damage and gut microbiota changes. *Microbiology Spectrum*, **12**: e03283–23.

Liu P, Yang JL, Chen Y, et al. 2023a. Alterations of gut microbiota and metabolome in early chronic kidney disease patients complicated with hyperuricemia. *Heliyon*, **9**(9): e20328.

Liu SQ, He YF, Zhang YL, et al. 2023b. Targeting gut microbiota in aging-related cardiovascular dysfunction: focus on the mechanisms. *Gut Microbes*, **15**(2): 2290331.

Magoč T, Salzberg SL. 2011. FLASH: fast length adjustment of short reads to improve genome assemblies. *Bioinformatics*, **27**(21): 2957–2963.

Marx PA, Maul DH, Osborn KG, et al. 1984. Simian AIDS: isolation of a type D retrovirus and transmission of the disease. *Science*, **223**(4640): 1083–1086.

Maul DH, Lerche NW, Osborn KG, et al. 1986. Pathogenesis of simian AIDS in rhesus macaques inoculated with the SRV-1 strain of type D retrovirus. *American Journal of Veterinary Research*, **47**(4): 863–868.

Ning M, An LN, Dong L, et al. 2024. Causal associations between gut microbiota, gut microbiota-derived metabolites, and Alzheimer's disease: a multivariable mendelian randomization study. *Journal of Alzheimers Disease*, **100**(1): 229–237.

Ogura H. 1980. Interactions among retroviruses Mason-Pfizer monkey, baboon endogenous, simian sarcoma virus-associated and murine leukemia detected by virus-mediated cell fusion inhibition assay. *Microbiology and Immunology*, **24**(8): 761–763.

Osborn KG, Prahalada S, Lowenstine LJ, et al. 1984. The pathology of an epizootic of acquired immunodeficiency in rhesus macaques. *The American Journal of Pathology*, **114**(1): 94–103.

Qian XH, Hai WX, Chen SY, et al. 2023. Multi-omics data reveals aberrant gut microbiota-host glycerophospholipid metabolism in association with

neuroinflammation in APP/PS1 mice. *Gut Microbes*, **15**(2): 2282790.

Reitz MS Jr, Wong-Staal F, Haseltine WA, et al. 1979. Gibbon ape leukemia virus-Hall's Island: new strain of gibbon ape leukemia virus. *Journal of Virology*, **29**(1): 395–400.

Ruchika, Bhardwaj N, Saneja A. 2024. Orally fast dissolving α-lipoic acid electrospun nanofibers mitigates lipopolysaccharide induced inflammation in RAW 264.7 macrophages. *International Journal of Biological Macromolecules*, **264**(Pt 1): 130623.

Schloss PD, Westcott SL, Ryabin T, et al. 2009. Introducing mothur: open-source, platform-independent, community-supported software for describing and comparing microbial communities. *Applied and Environmental Microbiology*, **75**(23): 7537–7541.

Sencio V, Machelart A, Robil C, et al. 2022. Alteration of the gut microbiota following SARS-CoV-2 infection correlates with disease severity in hamsters. *Gut Microbes*, **14**(1): 2018900.

Siriyasatien P, Intayot P, Chitcharoen S, et al. 2024. Comparative analysis of midgut bacterial communities in Chikungunya virus-infected and non-infected *Aedes aegypti* Thai laboratory strain mosquitoes. *Scientific Reports*, **14**(1): 10814.

Skibska B, Kochan E, Stanczak A, et al. 2023. Antioxidant and anti-inflammatory effects of α-lipoic acid on lipopolysaccharide-induced oxidative stress in rat kidney. *Archivum Immunologiae et Therapiae Experimentalis*, **71**(1): 16.

Tong YH, Cao YH, Jin TZ, et al. 2022. Role of interleukin-1 family in bone metastasis of prostate cancer. *Frontiers in Oncology*, **12**: 951167.

van der Kuyl AC. 2021. Contemporary distribution, estimated age, and prehistoric migrations of old world monkey retroviruses. *Epidemiologia*, **2**(1): 46–67.

Vieira AT, Baumert TF. 2024. The gut microbiome as a guidepost for infection risk in liver transplantation. *Cell Host & Microbe*, **32**(1): 9–11.

Wang HJ, Wang YJ, Yang LB, et al. 2024a. Integrated 16S rRNA sequencing and metagenomics insights into microbial dysbiosis and distinct virulence factors in inflammatory bowel disease. *Frontiers in Microbiology*, **15**: 1375804.

Wang JF, Liu JZ, Chang QM, et al. 2018. The association between preoperative serum interleukin-6 levels and postoperative prognosis in patients with T2 gallbladder cancer. *Journal of Surgical Oncology*, **117**(8): 1672–1678.

Wang Y, Zhang JQ, Wang XX, et al. 2024b. The inflammatory immunity and gut microbiota are associated with fear response differences in laying hens. *Poultry Science*, **103**(7): 103816.

Wheeler ML, Limon JJ, Bar AS, et al. 2016. Immunological consequences of intestinal fungal dysbiosis. *Cell Host & Microbe*, **19**(6): 865–873.

Xu LB, Yang YP, Li YD, et al. 2023. Characterizing the pathogenicity and immunogenicity of Simian Retrovirus Subtype 8 (SRV-8) using SRV-8-infected cynomolgus monkeys. *Viruses*, **15**(7): 1538.

Yang AM, Inamine T, Hochrath K, et al. 2017. Intestinal fungi contribute to development of alcoholic liver disease. *The Journal of Clinical Investigation*, **127**(7): 2829–2841.

Yang YP, Yu ML, Lu Y, et al. 2024a. Characterizing the rhythmic oscillations of gut bacterial and fungal communities and their rhythmic interactions in male cynomolgus monkeys. *Microbiology Spectrum*, **12**: e00722–24.

Yang Z, Song Y, Chen BT, et al. 2024b. Associations of gut and circulating microbiota with circulating vitamin D_3, type I interferon, and systemic inflammation in chronic spontaneous urticaria patients. *Journal of Inflammation Research*, **17**: 2775–2785.

Yee JL, Vanderford TH, Didier ES, et al. 2016. Specific pathogen free macaque colonies: a review of principles and recent advances for viral testing and colony management. *Journal of Medical Primatology*, **45**(2): 55–78.

Zao CL, Ward JA, Tomanek L, et al. 2011. Virological and serological characterization of SRV-4 infection in cynomolgus macaques. *Archives of Virology*, **156**(11): 2053–2056.

Zhu JT, Yang LY, Zhang QB, et al. 2020. Autophagy induced by simian retrovirus infection controls viral replication and apoptosis of jurkat T lymphocytes. *Viruses*, **12**(4): 381.